Materials Research. 2024; 27:e20230415
DOI: https://doi.org/10.1590/1980-5373-MR-2023-0415

Combined Effects of Nb Content, Thermal Parameters, and Dendritic Scale Length on Electrochemical Corrosion in Horizontally Solidified Al3CuxNb Alloys

Helder Rodrigues[a], Hugo Azevedo[b], Thiago Dillon[a], Gabriel Mendes[a], Evaldo Hoffmann[a], Bruno Feio[a], Jose C. Filho[b], Otavio L. Rocha[a,b]*

[a]*Instituto Federal de Educação, Ciência e Tecnologia do Pará (IFPA), 66093-020, Belém, PA, Brasil.*
[b]*Universidade Federal do Pará (UFPA), 66075-110, Belém, PA, Brasil.*

Received: September 22, 2023; Revised: January 07, 2024; Accepted: March 28, 2024

In this work, the effects of thermal solidification and microstructural parameters, such as solidification rate (V_L), cooling rate (T_R), and secondary dendritic spacing (λ_2), were studied on the electrochemical parameters of corrosion potential (E_{CORR}), current corrosion resistance (I_{CORR}), and polarization resistance (R_P). The alloys were solidified in a horizontal solidification device and two as-cast samples from the heat transfer surface were subjected to electrochemical polarization and impedance techniques. It was verified that the experimental values found for E_{CORR} were relatively close for all the investigated alloys and in both analyzed positions, allowing to deduce that the V_L, T_R and λ_2, as well as the Nb content had little influence, but enough to lead to different behavior in the I_{CORR} and R_P. For the alloy with 0.5wt.%Nb, higher V_L and T_R values, and smaller λ_2 resulted in lower I_{CORR} values. On the other hand, for alloys with 3 and 5wt.%Nb, coarser microstructures (greater λ_2) have lower corrosion rates. Microstructural analysis showed that Nb acts as a protective element against corrosive actions in the dendritic matrix.

Keywords: *Al-Cu-Nb alloys, Solidification thermal parameters, Microstructure, Corrosion resistance.*

1. Introduction

Aluminum has high stability when exposed to certain oxidizing environments, which can be attributed to the natural formation of an oxide layer (Al_2O_3) that works as a barrier to corrosion[1-8]. The electrochemical behavior of aluminum and its alloys is also influenced by this oxide layer, which forms spontaneously and governs their corrosion resistance. The rate of formation and the properties of Al_2O_3 depend on the chemical composition of the alloys and, therefore, the dissolution rate of the film will change with the addition of alloying elements to the metallic matrix. For example, magnesium enhances the protective properties of the oxide film of aluminum alloys forming mixed oxides which form 5XXX series alloys exhibit excellent corrosion resistance[1-8].

Despite the high resistance to corrosion, which may be associated with the presence of the passivation layer, aluminum alloys are subject to high current densities when subjected to aggressive media[4-13]. When in contact with the atmospheric environment, for example, it's highly resistant to corrosive processes, however, depending on the medium and condition to which it is exposed, this resistance will assume different behaviors since the aggressiveness of the medium can destroy the protective layer, leaving it vulnerable to corrosive processes[1-3]. Certain elements reduce these protective properties, as is the case with copper[3-8]. Al-Cu alloys are generally less corrosion resistant than other alloys. In these alloys, intermetallics of Al_2Cu, Al_2CuMg, and Al_7Cu_2Fe are some of those responsible for initiating galvanic corrosion with the matrix[4,5,7,8,12].

Electrochemical techniques such as open circuit potential (OCP), electrochemical potentiodynamic polarization (EPP) and electrochemical impedance spectroscopy (EIS) are efficient ways to analyze and monitor the corrosion resistance of metallic materials. The ease of obtaining data and the versatility of applications are some of the characteristics that make these techniques the most used ones in this type of investigation[14-40], which have been applied in different situations of corrosive environments, more or less aggressive, ranging from electrolytes such as NaCl[4,5,9,12,13,18,32,33,35,36,39,40], NaOH[22,25,26,28,38], HCl[15-18,20-24,27,29,31,41], and H_2SO_4[19,23].

The study of the solidification phenomenon of multicomponent casting alloys has provided the development of metallic materials with differentiated and increasingly specific properties. In real applications, the transient conditions in which this phenomenon occurs lead to several possibilities for obtaining final structures for the same cast product and, consequently, for its performance[4-9,12,13,42,43]. The effects of the alloying element, and of unsteady-state solidification conditions, such as growth and cooling rates (V_L e T_R), and the length of microstructural scales, were evaluated on the electrochemical characteristics of aluminum alloys[4-9,12,13]. Directional solidification experiments were carried out with Al-Cu[4,5,8,12], Al-Cu-Si[7], Al-Cu-Mg[4,5], Al-Cu-Ni[9] and Al-Si-Mg[6] alloys, and the results showed that the microstructure plays a fundamental role on the mechanical and corrosion

*e-mail: otavio.rocha@ifpa.edu.br

properties. The addition of Mg to an Al–Cu alloy has led to a considerable increase in Vickers Microhardness (HV), but reduced the corrosion resistance of the ternary Al-Cu-Mg alloy in a 0.5 M of NaCl solution[4].

In turn, the combined effects of solidification microstructure refining scale and T6 heat treatment conditions on corrosion behaviour and HV were evaluated in the respective alloys, and the results reported that in both as-cast and heat-treated samples the coarser dendritic microstructure showed lower corrosion current densities, and that heat treatment improved the corrosion resistance of the Al-Cu-Mg alloy[6]. In a study[8], it was depicted for as-solidified samples of Al-3wt%Cu alloy that due to lower V_L and T_R values and, consequently, higher λ_2 values the Al_2Cu intermetallic phase was more susceptible to the action of electrochemical corrosion phenomena in a 0.2 mol.L^{-1} solution of HCl.

Investigations have shown that horizontally solidified as-cast samples of Al-3wt.%Cu-2wt.%Si[7] and Al-7wt.%Si-0.3wt.%Mg[6] alloys have higher corrosion resistance for smaller secondary dendritic spacing (λ_2). In the as-cast microstructure of the directionally solidified Al-4.5wt.%Cu alloy, smaller dendritic and eutectic interphase spacing provided a more extensive distribution of the protective barrier to corrosive action, since the Al_2Cu particles were enveloped by the α phase (α_E) that acted as a protection against corrosion[12]. In the directionally solidified Al-3Mg-1Si alloy (wt.%) (for 0.15 M and 0.5 M in NaCl electrolytes)[13], better electrochemical behavior was observed for finer cellular and dendritic arrays, due to lower current densities and more positive corrosion potential when compared with coarser microstructures.

In our recent studies, the effects of the solidification thermal parameters and the T6 heat treatment were evaluated on the length of the microstructural scale and on the microhardness HV[42,43], as well as on the electrical conductivity of the investigated alloys in this work[42]. However, there is still a need for studies that seek to understand the influence of thermal and microstructural parameters on the corrosion resistance of Al-3Cu-xNb alloys (x=0.5, 3 and 5wt.%), which is the main focus of investigation of this work, aiming to add new scientific knowledge to the development chain of the respective alloys.

In this sense, observing the continuous development of research pertinent to niobium and its importance to Brazil, aiming to deepen these studies, the main goal of this investigation is to evaluate the effects of thermal parameters, microstructure and Nb composition, mainly regarding the role of the Al_2Cu and Al_3Nb intermetallic phases, on electrochemical characteristics, such as potentiodynamic polarization and electrochemical impedance spectroscopy (EIS), in two samples in the as-cast ingot from the heat transfer surface of horizontally solidified Al-3Cu-xNb (x=0.5, 3 and 5wt.%) alloys.

2. Materials and Methods

Horizontal solidification experiments were carried out with Al-3Cu-xNb alloys (x=0.5, 3 and 5wt.%) in our recent work[42,43], and in order to evaluate the combined effects of Nb and microstructural scale length on corrosion resistance of the aforementioned alloys, samples of solidified ingots were submitted in this work to electrochemical tests.

The casting assembly used in the horizontal solidification experiments is shown in Figure 1. The solidification device was designed in such a way that heat was extracted only through one water cooled side, thus promoting solidification along the longitudinal length of the rectangular mold, as can be seen in Figure 1a. In order to perform a thermal analysis and determine the investigated solidification thermal parameters (V_L and T_R), continuous measurements of temperatures in the melts were monitored during solidification through

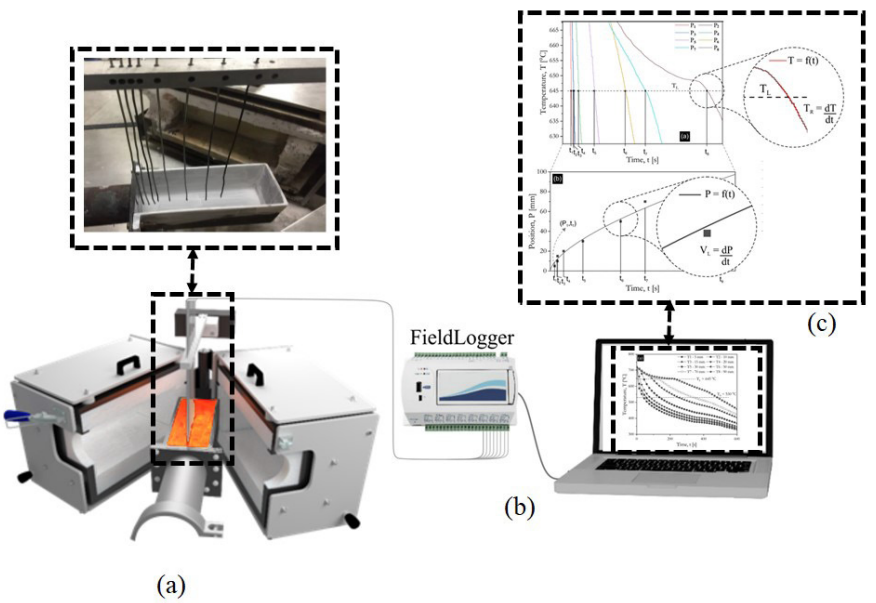

Figure 1. Schematic representation of horizontal experimental solidification assembly: (a) HS device, (b) thermal data acquisition system, and (c) technique for determining of V_L and T_R.

the output of a group of thin type K thermocouples coated in stainless steel tubes of 1.6 mm outside diameter and strategically positioned in respect to heat extraction surface on the cooled part of the ingot mold, as shown in Figure 1b. All the thermocouples were connected by coaxial cables to a data logger interfaced with a computer, and the temperature data was acquired automatically. Once the thermal data was generated, the experimental V_L and T_R values were determined, as shown Figure 1c. More details on this experimental set-up can be found in a previous articles[4-8,42,43].

Figure 2 illustrates one of the ingots of the investigated alloys, showing how subsequent cuts were performed to obtain samples for microstructural characterization and electrochemical tests. Selected longitudinal sections of the solidified ingot were polished and etched with Keller's reagent (10ml of HF, 15ml of HCl, 25ml of HNO_3 and 50ml of H_2O) to reveal the microstructure, as shown in Figure 2a, as well as two as-cast samples were selected for each alloy in the cross section at positions 10 and 70 mm from the cooled base to carry out the electrochemical tests, as can be seen in Figure 2b. The length of the microstructural scale was analyzed by measuring the secondary dendritic spacing, as shown in Figure 2c.

MOTIC and the image processing software ImageJ were used to measure the secondary dendrite arm spacings, and at least 20 measurements were taken for each selected position along the casting length. Furthermore, a scanning electron microscope (SEM TESCAM, VEGA LMU) coupled to an energy dispersion spectrum (EDS X-MAX 20, Oxford) was used to investigate the microstructural phases of the samples before and after the corrosion tests.

Figure 3 shows the schematic procedure of the experimental assembly used for the application of the electrochemical tests. Initially, in an electrolytic cell (4), 500 mL of 0.2 mol.L^{-1} of HCl solution was added at room temperature of 25°C. For the electrochemical measurements, a system of three electrodes (5), (6) and (7) was used for each test, fixed by electrical terminals (3) interconnected to the potentiostat/galvanostat (2), both connected to the microcomputer (1) with ESA 400 software from Gamry Instruments to obtain and analyze the anodic and cathodic potentiodynamic polarization curves and potential of corrosion. In addition to visualization, interpretation and adjustment of Nyquist diagrams obtained by electrochemical impedance spectroscopy. These electrochemical measurements during the corrosion process were obtained in accordance with the technical standard ASTM G3-14 [44].

Aiming to develop a comparative study with works based on literature[7,8], all electrochemical experiments were performed in HCl 0.2 M at room temperature. The use of HCl is justified by the fact that it is a strong inorganic acid, with a very low pH (~0.7) and easily ionizable in aqueous solutions. When it reacts with aluminum, it produces substantial loss of the metal through corrosion, where chloride ions (Cl-) attack the metal surface forming aluminum chloride ($AlCl_3$) and releasing hydrogen (H_2(g)). HCl solution is one of the most currently used acids in the pickling and electrochemical etching of aluminum capacitor foil, and it is widely used for acid cleaning and electro-polishing of aluminum. In addition, the passive Al_2O_3 layer is inert in most environments and resistant to a wide variety of chemical agents, however it is susceptible to hydrochloric acid (HCl) solutions that are used in acid pickling, a surface treatment of metals such as aluminum and its alloys[6]. More details on the preparation and execution of electrochemical tests can be consulted in our recent research[6-8].

3. Results and Discussion

3.1. Heat flow parameters

Results of thermal analysis, including heat flux parameters, active in the solidification process, such as temperature records as well as growth and cooling rates (V_L and T_R),

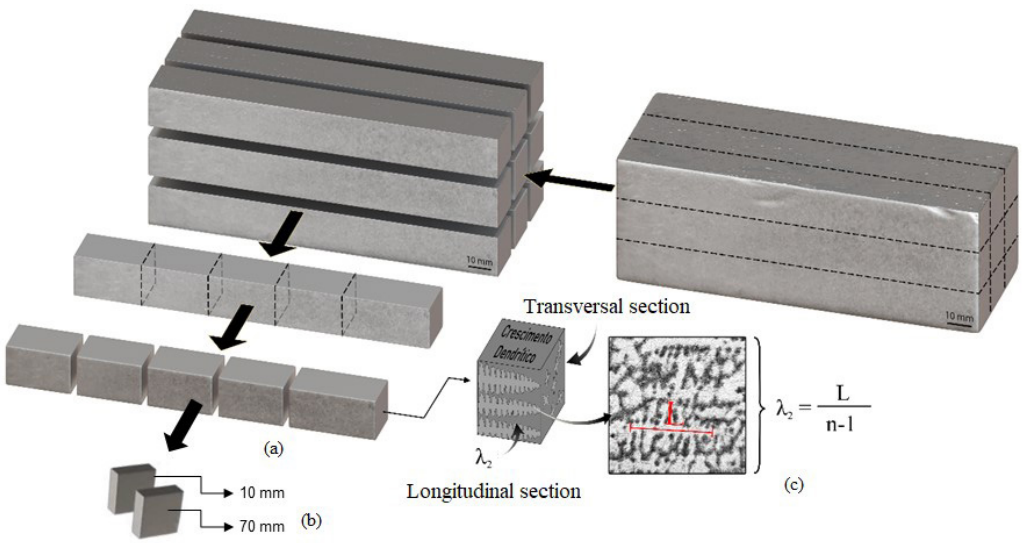

Figure 2. Illustration of the procedure for cutting solidified samples for microstructural analysis and electrochemical tests: (a) and (b) longitudinal and transverse sections, and (c) λ_2 measurement technique. Source: Adapted from Mendes et al.[42].

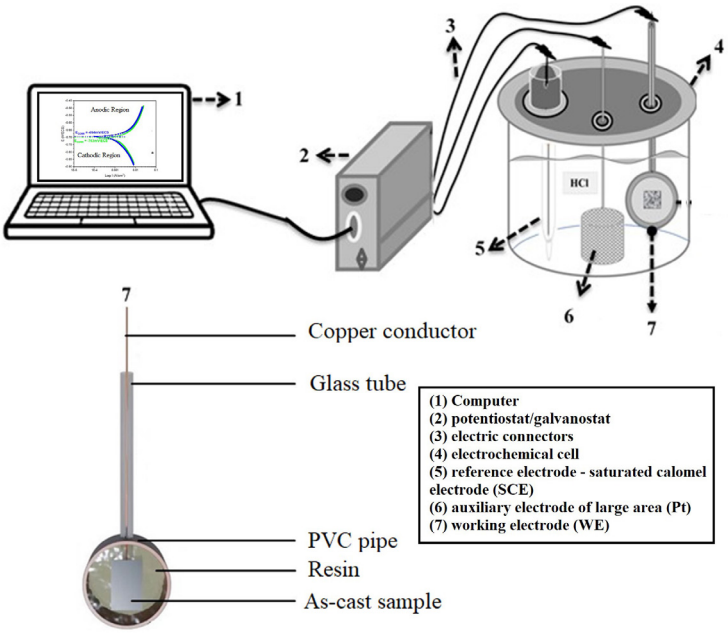

Figure 3. Schematization of the assembly of materials and equipment for carrying out the electrochemical test. Source: Adapted from Soares et al.[8].

were discussed in our recently published studies[42,43], which have been used in this work to establish a correlation with the electrochemical corrosion parameters. Thus, typical plots of experimental cooling curves for thermocouples placed along the length of castings resulting from horizontal solidification (HS) (see Figures 1a and 1b) of Al-3wt.%Cu-xNb alloys (x=0.5, 3 and 5wt. %) were used to determine the thermal solidification parameters (V_L and T_R), according to the methodology in Figure 1b, whose results can also be seen in our recent research[42,43]. Mathematical expressions have been proposed to predict the V_L and T_R variation along the length of the solidified ingot (P), given by $V_L=C_1(P)^n$ and $T_R=C_2(P)^m$ according to Table 1. It was verified that the use of a water-cooled mold imposes higher growth and cooling rates values of Al-rich phase dendrite tips in positions (P) close to the heat transfer surface (cooled base of the ingot), and a decreasing profile of V_L and T_R along the length of the as-cast ingot due to the increase in the thermal resistance of the solidification layer with distance from the aforementioned cooled base.

In our recent research[42,43], with the same investigated alloys and solidification conditions as in the present work, the results showed that the microstructure revealed for the Al-rich phase along the length of the solidified ingot was constituted predominantly by a dendritic network.. In these studies, thermal analysis for non-equilibrium and very close to equilibrium conditions, as well as the typical solidification microstructures showed, during the solidification path, the occurrence of a peritectic reaction represented by Liquid + $Al_3Nb \rightarrow Al_\alpha$ for the Al-3Cu-xNb alloys (x=3 and 5wt .%), in which the primary Al_3Nb intermetallic phase was observed surrounded by Al-rich dendritic phases (Al_α). Both V_L and T_R were considered as the growth and cooling rates that governed the growth of secondary dendritic branches. Thus,

Table 1. Experimental results of the solidification thermal parameters for the investigated alloys.

Alloy (Al-3Cu-xNb) (wt.%)	$V_L=f(P)$	$T_R=f(P)$
x=0.5	C_1 = 2.17 and n = -0.30	C_2 = 82.2 and m = -0.70
x=3	C_1 = 1 and n = -0.25	C_2 = 34.46 and m = -0.73
X=5	C_1= 3.4 and n = -0.56	C_2 = 43.82 and m = -0.78

the effects of thermal parameters were evaluated on the length of the dendritic scale (Al_α) for the three horizontally solidified Al-3Cu-xNb alloys. As expected, finer dendritic microstructures, represented by smaller λ_2 were achieved for positions closer to the heat transfer surface, whose ingot positions had the highest V_L and T_R values, as well as reported in the experiments of directional solidification of the references[9,12,13,35,36]. Power-type mathematical expressions were proposed, given by $\lambda_2=10.1(P)^{0.36}$, $\lambda_2=23(V_L)^{-2/3}$, and $\lambda_2=55.3(T_R)^{-1/3}$ .They characterize the λ_2 variation as a function of these solidification parameters, and the λ_2 values in the as-cast samples selected for the electrochemical tests are consolidated in Table 2. It was noted that the Nb content did not influence the growth laws of secondary dendritic spacing.

3.2. Electrochemical Measurements

3.2.1. Open circuit potential

The study involves changing the potential of the working electrode and monitoring the current that is produced as a function of time or potential. The corrosion potential (E_{OC}) variations under open circuit potential (OCP) condition with time graphs recorded in 0.2 mol.L^{-1} HCl solution for all the three types of specimens and two positions (10 and

70 mm) are shown in Figure 4a. In the initial moments, the E_{OC} curves for all alloys showed equal characteristics with profiles far apart in the two as-cast positions studied and descending in the first 100 s, and that after this time they grew and stabilized from 600 s, reaching the final values at time equal to 1200 s. Except for the first 100 s, similar open circuit potential behaviors are found in the literature for other aluminum alloys subjected to the same working electrolyte (HCl)[6-8,45]. The observed trend indicates minimum shift of the E_{OC} in the negative potential direction and turning to achieving the plateau region after 600 s of exposure for all the investigated specimens. This movement towards less electronegative regions can be explained by the reduction of the active area due to the formation of a protective oxide layer on the metal surface. The initial spacing and then approximation of the curves and E_{OC} values may indicate that the composition and behavior of the passive films during acid immersion are similar. As can be seen, the final E_{OC} measurements indicated different values for both positions, demonstrating that the solidification parameters, represented by V_L, T_R and λ_2, as well as the Nb composition, exerted a strong influence on the electrochemical behavior. It was observed that for contents of 0.5 and 3wt.%Nb, lower E_{OC} values were found for a position equal to 10mm compared to a position equal to 70 mm from the refrigerated mold plate, that is, corresponding to higher and lower T_R and V_L values, whose positions secondary dendritic spacing assumed values equal to 23.4 and 46.61µm, respectively.

The comparative study shown in Figure 4b has indicated more electronegative E_{OC} values for the ternary Al-3Cu-xNb (wt.%) and Al-3Cu-2Si wt.%[7] alloys in relation to the values found for the binary Al-3wt. %Cu alloy[8]. This can be attributed to the presence of intermetallic phases within the interdendritic regions of ternary alloys with high corrosion potential, as reported in[4-8,40].

3.3. Polarization measurements

Through the potentiodynamic polarization test, it is possible to determine both the corrosion current density (I_{CORR}) and the corrosion potential (E_{CORR}), parameters of fundamental importance, since the corrosion rate is directly proportional to the corrosion current density, so it is often used in electrochemical corrosion analysis[4,5]. Thus, the effect of hydrochloric acid on the corrosion rate (I_{CORR}) of as-cast samples in the two studied positions, 10 and 70mm, of Al-3Cu-xNb alloys (x=0.5, 3 and 5wt.%Nb), was investigated by the method of Tafel extrapolation. The anodic and cathodic polarization curves obtained for the aforementioned ternary alloys in an acid medium of HCl 0.2M are shown in Figure 5a. In general, the polarization results shown in Figure 5a for all Nb compositions indicate that the behavior of the anodic and cathodic curves was similar in both studied solidification positions.

For all the investigated alloys, small displacements of the curves were noticed in relation to the positions in the ingot, that is, in the Al-3wt.%-0.5wt.%Nb alloy the anodic and cathodic curves, position equal to 70 mm, suffered

Table 2. Simulated experimental values for V_L and T_R from data presented in Table 1, and λ_2=f(P).

Alloy (Al-3Cu-xNb) (wt.%)	Position (mm)	V_L (mm/s)	T_R (°C/s)	λ_2 (µm)
x=0.5	10	1.01	16.4	23,13
	70	0.60	4.20	46.61
x=3	10	0.56	6.42	23.13
	70	0.34	1.60	46.61
x=5	10	0.93	7.30	23.13
	70	0.31	1.60	46.61

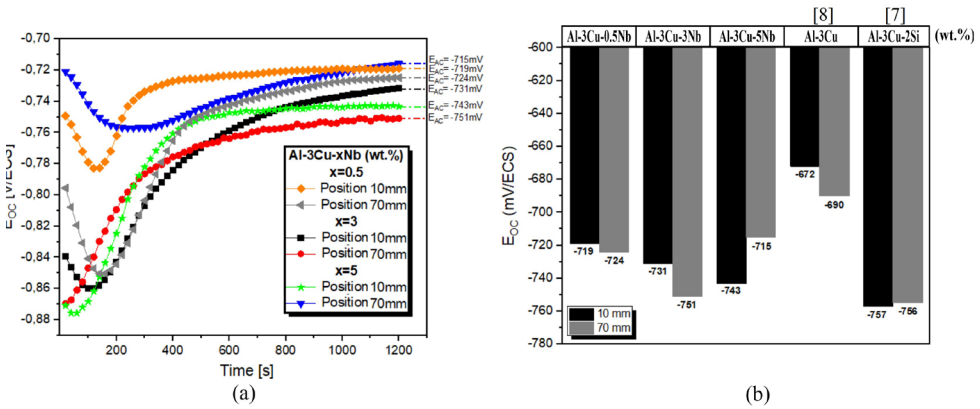

(a) (b)

Figure 4. (a) Experimental open circuit potential (E_{OC}) curves as a function of time for the searched alloys in 0.2 M HCl at two positions, 10 and 70mm, from the heat transfer surface, and (b) comparison conducted with works from the literature.

a small displacement to the right, while for the other Nb compositions (3 and 5wt.%) the displacement to the right was observed in the curves of the position equal to 10 mm. Such behaviors allowed observing differences in the results of the electrochemical parameters, potential and corrosion density (E_{CORR} and I_{CORR}), as shown in Figure 5b.

In concomitant observation between Figures 4 and 5, values close to E_{CORR} and E_{OC} were found, thus demonstrating the effectiveness of the electrochemical tests carried out under the assumed conditions. It was verified that the experimental values found for E_{CORR} were relatively close for all the investigated alloys and corresponding positions analyzed, allowing to deduce that they can assume values ranging from -694 to -711mV, and that the solidification parameters (V_L, T_R and λ_2) as well as the Nb content have little influences, as shown in Figure 5b, but enough to drive different behaviors in the corrosion rate (I_{CORR}), as can be evidenced in Figure 5c. Different effects of solidification thermal and microstructural parameters on I_{CORR} have been observed, since for the content of 0.5wt.%Nb, higher V_L and T_R, and lower λ_2 resulted in lower I_{CORR}, but for higher Nb compositions (3 and 5wt.%), coarser microstructures (higher λ_2) have lower corrosion rates.

Figures 5b and 5c present a comparative study with the Al-3Cu-2Si alloy (wt,%)[7] solidified under the same solidification conditions of this work. As can be seen, the alloys investigated in this work showed greater resistance to corrosion due to lower corrosion rates (I_{CORR}). Studies with the Al-3wt.%Cu-2wt.%Si alloy[7] pointed to the interference of silicon in the composition of the eutectic mixture with the intermetallic phase Al_2Cu in increasing the rate of the interdendritic corrosive process in an acidic medium of HCl

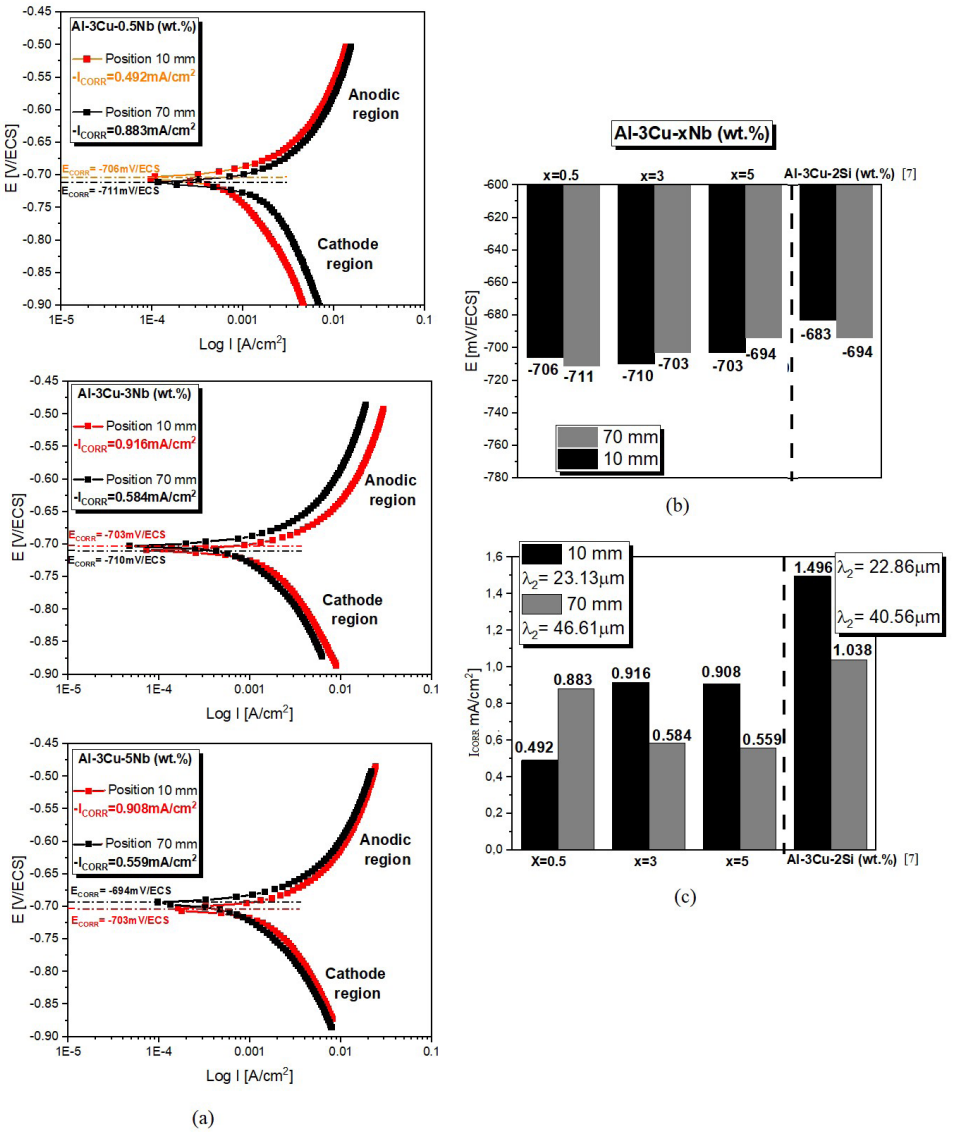

Figure 5. (a) Potentiodynamic polarization curves for Al-3Cux-Nb alloys in 0.2 M of HCl obtained for the two studied samples, 10 and 70 mm from the heat transfer interface, and (b) and (c) represent the electrochemical parameters, E_{CORR} e I_{CORR}, respectively, determined by Tafel.

0.2 mol.L^{-1}. The increase in Nb content, consequently, and the length of the scale of the microstructure play a key role in corrosion resistance. Studies observed that finer dendritic spacing leads to a more homogeneous distribution of Al_2Cu, contributing to the increase in corrosion resistance[46]. On the other hand, for the Al-Si alloy greater corrosion resistance has been attributed to higher λ_2 values due to the dissimilar growth behavior between the dendritic matrix and the eutectic Si crystals, which causes localized tensions[46]. Table 3 consolidates the results obtained E_{CORR}, I_{CORR}, and anodic (b_a) and cathodic (b_c) inclinations from Tafel extrapolations, compared with values from the literature[7]. The achieved values of b_a (47.7 to 54.5) and b_c (108.31 to 121.1) for the alloys in this work indicate that they did not cause changes in the reaction mechanism of the corrosion process. It is important to highlight that these values are among those proposed for the Al-3Cu-2Si (wt.%) alloy[7].

3.4. Electrochemical impedance measurements

In this work, analysis by electrochemical impedance spectroscopy was also carried out, with the option of presenting the results in Nyquist graphical form, with real impedance values on the abscissa and imaginary values on the ordinate, as shown in Figure 6a. The Nyquist diagrams are presented as semicircles indicating that the corrosion process is mainly governed by charge transfer with only a capacitive loop at high frequencies and the onset of a small inductance at lower frequencies. Similar impedance characteristics have been reported in the literature for aluminum alloys in various electrolytes such as sulfuric acid, sodium chloride and composite solutions[41,47-49]. The impedance results used to characterize the HCl corrosion of the Al-3Cu-xNb alloys (x=0.5, 3 and 5wt.%) in the ingot positions at 10 and 70 mm were obtained after 2 h of immersion in the working electrolyte. The equivalent electrical circuit used in the modeling is presented in Figure 6b, in which the circuit components and the corresponding Nyquist diagram system are illustrated. This model is applied to spectra that present characteristics close to a semicircle.

Thus, through polarization resistance (R_p) and electrolyte/solution resistance (R_{el}), real data of high and low impedance frequencies were calculated, in which the real axis is intercepted by the spectra, considering the difference between these values to obtain R_p, these data are consolidated in Table 4, which presents the Rp and R_{el} values in series with capacitance elements (C_{dl}).

In the presented curves, it was observed that the resistive behaviors highlighted, for the two positions in all the alloys investigated, revealed similar impedance characteristics with spectra in a semicircle format, indicating that the reaction mechanism remains unaltered. Despite the similarity of behavior, the results indicated for all studied compositions that the sample in the position 10mm (close to the heat transfer surface), where higher V_L and T_R were found, and λ_2 has been smaller, have presented lower impedance diameters at all data acquisition points during the time of the experiment. These results clearly demonstrate that the polarization resistance in the position of 70 mm, that is, for coarser microstructures, was superior to that in the position of 10 mm (small λ_2) in the used electrolyte[7]. Higher polarization resistance values were also found for coarser microstructures in Al-3Cu-xMg (x=0 and 0.5wt.%) alloys[4] after corrosion

Table 3. Electrochemical parameters obtained by Tafel extrapolation for the Al-3%Cu-x%Nb alloy immersed in 0.2 mol.L^{-1} HCl at 25°C.

Alloy (Al-3Cu-xNb) (wt.%)	Position (mm)	E_{CORR} (mV/ECS)	I_{CORR} (mA/cm^2)	Tafel slope (mV)	
				b_a	b_c
x=0.5	10	-706	0.492	54.45	121.12
	70	-711	0.883	72.32	108.31
x=3	10	-710	0.916	47.7	115
	70	-703	0.584	56.4	104
X=5	10	-703	0.908	56.48	106.58
	70	-694	0.559	42.5	113.34
Al-3Cu-2Si (wt.%)[7]	10	-683	1.496	90,8	129.3
	70	-694	1.038	84,1	117.9

Table 4. Electrochemical impedance parameters obtained by simulation with corresponding equivalent circuit.

Alloy (Al-3Cu-xNb) (wt.%)	Position (mm)	R_{el} (Ω.cm^{-2})	R_p (Ω.cm^{-2})	C_{dl} (mF.cm^{-2})
x=0.5	10	11.51	24.39	8.78x10^{-4}
	70	9.46	27.57	6.28x10^{-4}
X=3	10	6.72	29.45	3.97x10^{-4}
	70	10.67	32.14	4.74x10^{-4}
X=5	10	8.64	23.02	8.63x10^{-4}
	70	9.38	34.25	4.44x10^{-4}

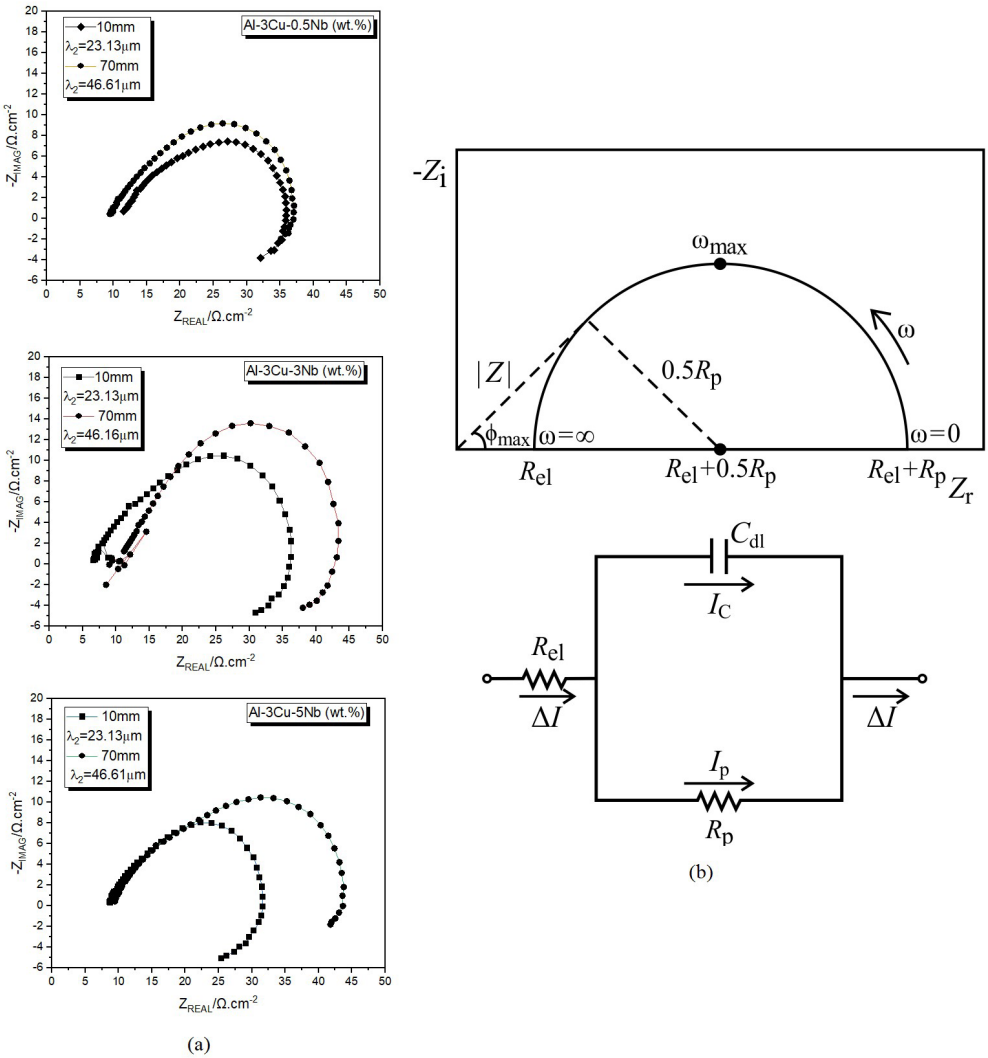

Figure 6. Experimental Nyquist diagrams for the searched alloys in 0.2 M HCl at two positions, 10 and 70mm, from the heat transfer surface, and (b) equivalent circuit diagram.

tests in 0.5 M NaCl solution, but for the Al-3%Cu-3.2%Si[7], under the same conditions as this work, with results shown in Figure 7, the most fine microstructure was the one that presented the greatest resistance to polarization.

3.5. Typical Solidified and corroded - like Microstructures

Figures 8 to 10 show typical SEM micrographs with point microanalysis by EDS of investigated as-cast samples (70 mm from the heat transfer surface) of the Al-3Cu-xNb (x=0.5, 3 and 5wt.%) alloys before and after the corrosion tests for 24 h in 0.2M of HCl solution. In general, predominant localized corrosion in the interdendritic zones can be observed, characterized by a higher concentration of oxygen that surrounds the Al_2Cu intermetallic particles, as can be evidenced by the results of the microanalyses of elements represented by points 2 and 3 in Figure 8, and points 3 in Figures 9 and 10.

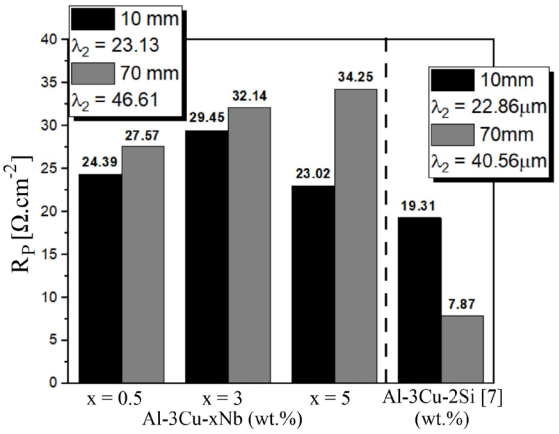

Figure 7. Polarization resistance (Rp) as a function of time for the Al-3Cu-xNb alloys (x=0.5, 3 and 5wt%) at two positions, 10 and 70mm, from the heat transfer surface.

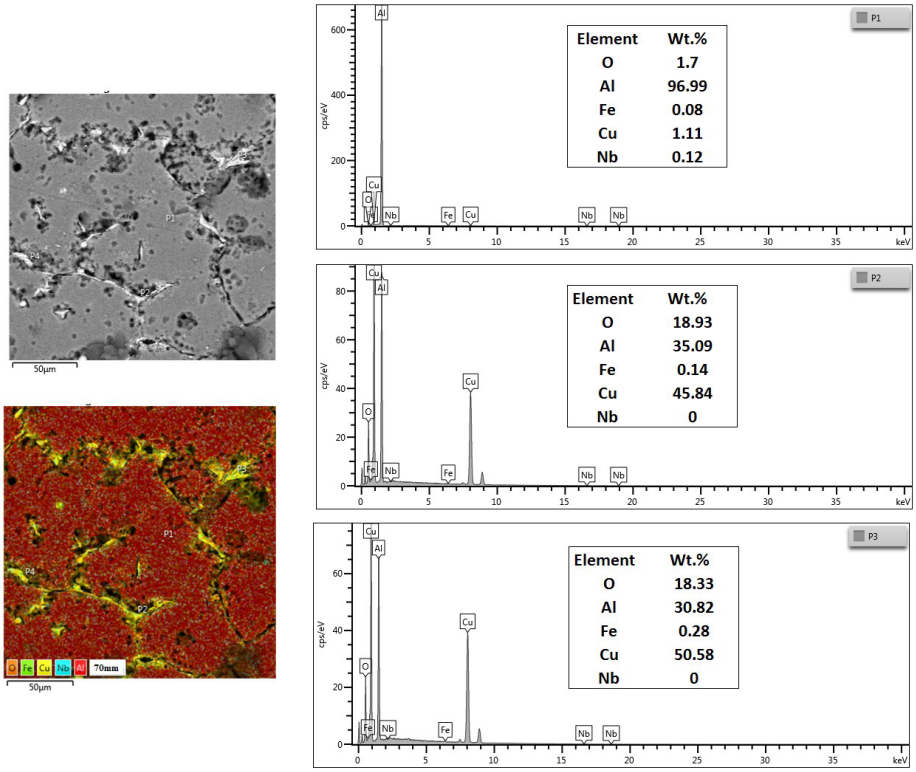

Figure 8. SEM/EDS micrographs for Al-3Cu-0.5Nb (wt.%) at position 70mm in the as-cast ingot from the heat extraction interface, after immersion in HCl (0.2 mol.L^{-1}) for 24 h.

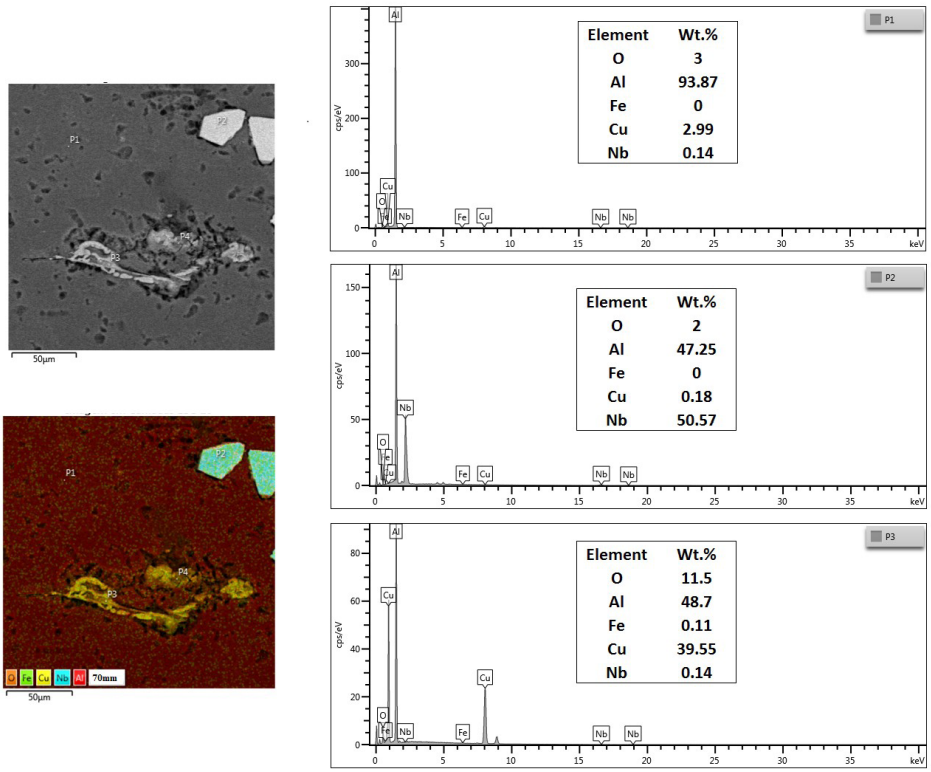

Figure 9. SEM/EDS micrographs for Al-3Cu-3Nb (wt.%) at position 70mm in the as-cast ingot from the heat extraction interface, after immersion in HCl (0.2 mol.L^{-1}) for 24 h.

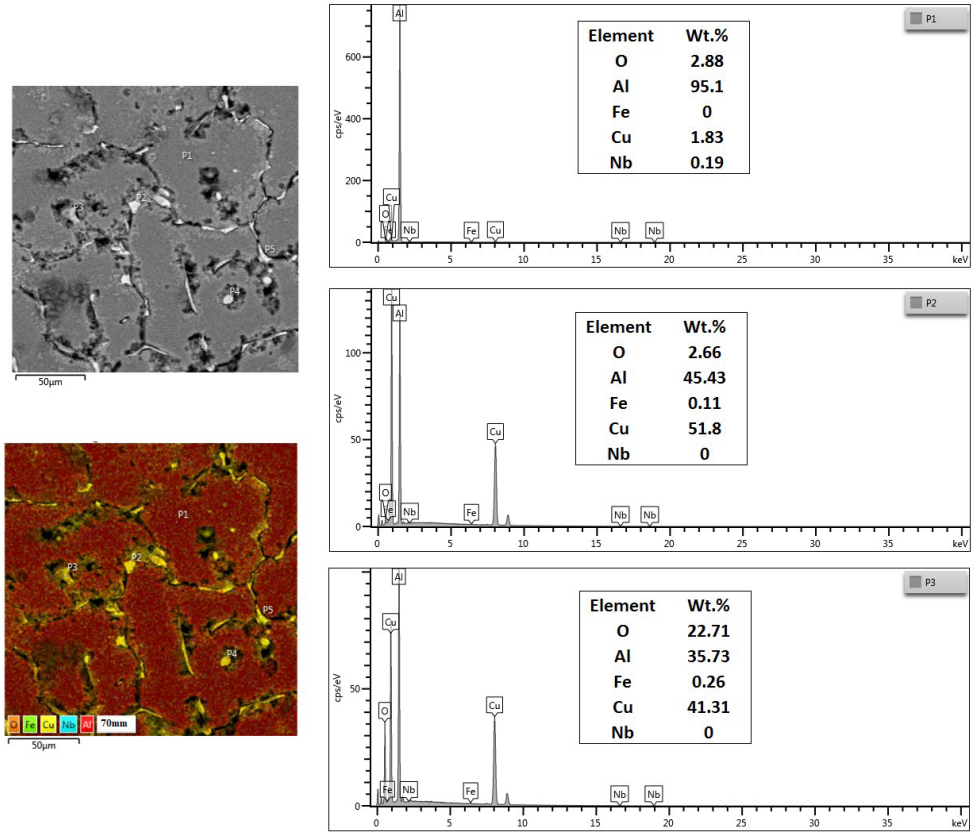

Figure 10. SEM/EDS micrographs for Al-3Cu-5Nb (wt.%) at position 70mm in the as-cast ingot from the heat extraction interface, after immersion in HCl (0.2 mol.L^{-1}) for 24 h.

The simulated and experimental solidification paths of the Al-3Cu-xNb alloys investigated in the present work were reported by Dillon et al[43] and Mendes et al.[42], and during cooling a peritectic reaction was observed for 3 and 5wt.%Nb contents, represented by Liq + Al_3Nb → Alα[42]. Experimental XRD patterns for the Al-3Cu-5Nb (wt.%) alloy investigated in this work were presented, and intensities/cps of Alα as well as the intermetallic phase Al_2Cu were noted in the XRD patterns, but peaks of Al_3Nb were not detected due to the low fraction of this phase which is partially consumed during the peritectic reaction (Liq + Al_3Nb→ Alα)[50]. On the other hand, thermal DSC and microstructural SEM/EDS analysis revealed the presence of Al_3Nb [50], as well as XRD analysis results showed Al_3Nb intermetallic intensities in upward solidified Al-xNb alloys (x=0.8 and 1.2wt.%Nb)[51].

In this work, the primary Al_3Nb-intermetallic phase has its presence confirmed in the microstructure surrounded by the Al-rich phase (Al_α), as can be seen from the element microanalysis performed on point 2 in Figure 9. This intermetallic appears to act as a protective phase of the Al_α matrix against electrochemical corrosion caused by the effects of the galvanic pile that occurs between the matrix and the Al_2Cu-intermetallic phase contained in the interdendritic eutectic mixture. In a comparative analysis with the Al-3wt.%Cu-2wt.%Si alloy[7], shown in Figure 7, the dissolved Nb in the matrix in the Al-3wt.%Cu-0.5wt.%Nb alloy as well as forming the intermetallic Al_3Nb in the Al-3Cu-xNb alloys (x=3 and 5wt.%), seems to act as a protective phase of the Al matrix against electrochemical corrosion caused by the effects of the galvanic pile that occurs between the Al_α-Al_2Cu and Al_α-(Al_2Cu+Si) contained in interdendritic eutectic mixtures of Al-Cu and Al-Cu-Si alloys, respectively. Intermetallic phases within the intendendrite regions in Al alloys can perform functions as a cathode during the corrosion process, as they are more noble than the Al-rich matrix[4-8,40], since the aluminum matrix around these eutectic phases was dissolved in the form of ions, i.e, suffered corrosion in greater proportions when compared to the interdendritic region, as shown in Figures 8 to 10.

Figures 11 to 13 show typical optical micrographs of the two studied samples of all alloys, after solidified and immersion for 24 h in a 0.2 M HCl solution. As can be seen, localized corrosion in the interdendritic regions and in the Al-rich matrix (a) can be observed, as also noted in[4-8]. It has been more intensely evidenced for alloys with low Nb content, especially in the Al-3C-0.5Nb alloy (wt.%), as shown in Figure 11. This has reinforced that Nb acts as a protective element against corrosive actions in the Al-rich matrix.

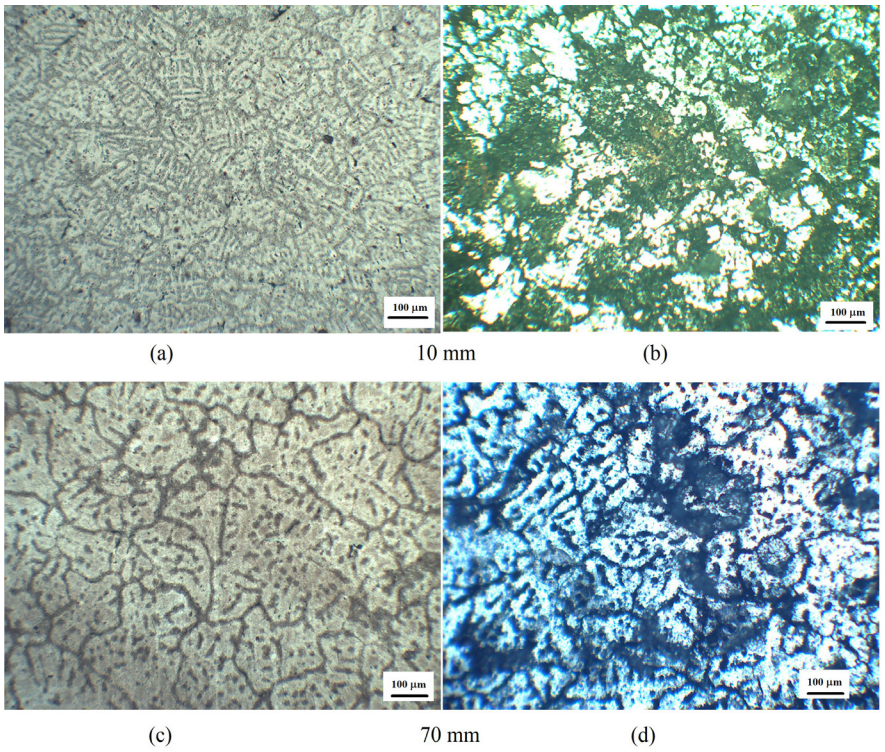

Figure 11. Microstructures of Al-3Cu-0.5Nb (wt.%) alloy in the two investigated positions: (a) and (c) solidified-like samples, and (b) and (d) after 24 hour immersion time in 0.2 M HCl solution.

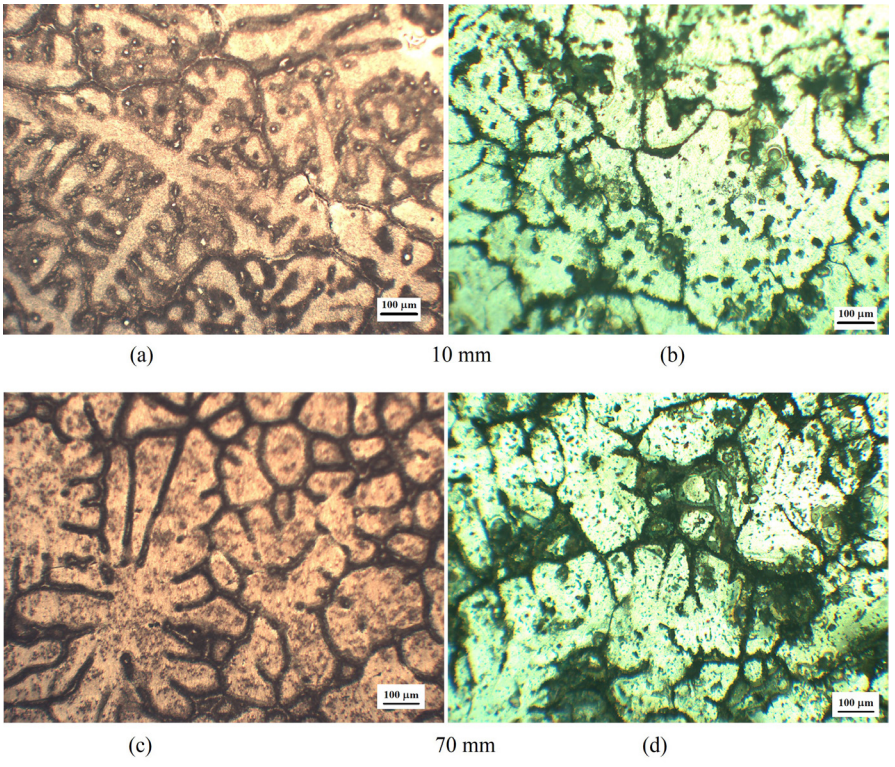

Figure 12. Microstructures of Al-3Cu-3Nb (wt.%) alloy in the two investigated positions: (a) and (c) solidified-like samples, and (b) and (d) after 24 hour immersion time in 0.2 M HCl solution.

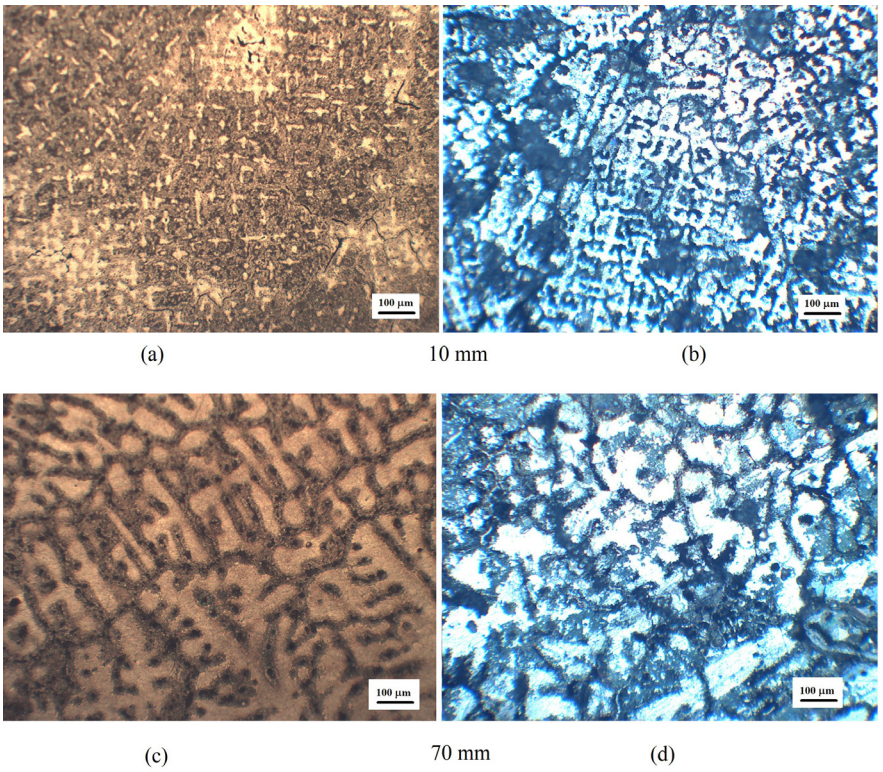

Figure 13. Microstructures of Al-3Cu-5Nb (wt.%) alloy in the two investigated positions: (a) and (c) solidified-like samples, and (b) and (d) after 24 hour immersion time in 0.2 M HCl solution.

4. Conclusions

The following conclusions have been derived from the present investigation:

(1) E_{OC} values found for the investigated alloys indicated that the composition and behavior of passive films during immersion in 0.2M of HCl were similar. It was observed that V_L, T_R and λ_2, as well as the Nb composition, exerted a strong influence on the electrochemical behavior.

(2) The potentiodynamic polarization test results for all Nb compositions showed that the behavior of the anodic and cathodic curves was similar in both as-cast positions. Given the solidification conditions assumed for the investigated alloys, it was verified that the experimental values found for E_{CORR} were relatively close, allowing to assume values ranging from -694 to 706mV, and that the solidification parameters (V_L, T_R and λ_2) as well as the Nb composition had little influence, but enough to lead to different performance in the corrosion rate (I_{CORR}). Different effects of the thermal solidification parameters and the length of the microstructural scale on the I_{CORR} were observed, that is, higher V_L and T_R, and smaller λ_2 for the content of 0.5wt%Nb resulted in lower I_{CORR}, while the opposite behavior was noticed for higher Nb contents (3 and 5wt.%) assumed in the investigated alloys.

(3) Analysis by electrochemical impedance spectroscopy in the Nyquist plot represented by semicircles showed that the corrosion process is mainly governed by charge transfer with only a capacitive loop at high frequencies and the onset of a small inductance at low frequencies, and revealed similar impedance characteristics with spectra in a semicircle format, indicating that the reaction mechanism remains unaltered.

(4) It was also observed that the solidification parameters, under the assumed conditions, imposed a fundamental role in the behavior of the electrochemical polarization resistance (R_P), since a more accentuated corrosive process was observed for higher V_L and T_R values, and smaller λ_2.

(5) The SEM/EDS analysis showed predominantly localized corrosion in the interdendritic regions of all investigated alloys, in which a higher concentration of oxygen enveloped Al_2Cu intermetallic particles. In addition, spot EDS microanalysis indicated the presence of the primary Al_3Nb intermetallic phase surrounded by a dendritic network characterized by the Al-rich phase (Al_α), which seemed to act as protective phases of the Al_α matrix against electrochemical corrosion due to the Al_2Cu intermetallic contained within the interdendritic region.

(6) Finally, Nb as dissolved in the matrix forming a solid solution Alα, as well as forming the Al_3Nb-type intermetallics, seems to act as a protective phase against the deleterious effects of corrosion on the dendritic network, caused by the cathodic behavior

of the Al_2Cu contained in the interdendritic region. Thus, the highest R_p values achieved in the alloys of this work when compared with those in the literature for the Al-3%Cu-3.2%Si alloy, seem to indicate that Nb acts to delay the corrosive process in the matrix.

5. Acknowledgments

The authors acknowledge the financial support provided by IFPA-Federal Institute of Education, Science and Technology of Pará, Postgraduate Program in Materials Engineering (PPGEMat/IFPA), UFPA-Federal University of Pará, CNPq-National Council for Scientific and Technological Development, Brazil, (Grant: 304924/2020-2), and CAPES – Coordenação de Aperfeiçoamento de Pessoal de Nível Superior- Brasil (PDPG/CAPES (Processo: 88881.707312/2022-01).

6. References

1. Hatch JE, editor. Aluminum: properties and physical metallurgy. Ohio: ASM International; 1984.
2. Davis JR, editor. Corrosion of aluminum and aluminum alloys. Ohio: ASM International; 1999.. http://doi.org/10.31399/asm.tb.caaa.9781627082990.
3. Vargel C, editor. Corrosion of aluminum. Paris: Elsevier Ltda.; 2004.
4. Barros A, Cruz C, Silva AP, Cheung N, Garcia A, Rocha O, et al. Horizontally solidified Al–3 wt%Cu–(0.5 wt%Mg) alloys: tailoring thermal parameters, microstructure, microhardness, and corrosion behavior. Acta Metall Sin. 2019;32:695-709.
5. Barros A, Cruz C, Silva AP, Cheung N, Garcia A, Rocha O, et al. Length scale of solidification microstructure tailoring corrosion resistance and microhardness in T6 heat treatment of an Al–Cu–Mg alloy. Corros Eng Sci Technol. 2020;55(6):471-9. http://doi.org/10.1080/1478422X.2020.1742410.
6. Barbosa CR, Silva TC, Azevedo HM, Cardoso JCA Fo, Moreira AL, Rocha OL. Correlation between unsteady-state solidification and electrochemical corrosion parameters of an AlSiMg alloy. Int J Met Cast. 2022;16(1):191-203. http://doi.org/10.1007/s40962-021-00571-1.
7. Silva TC, Barros AS, Cardoso JCA Fo, Moreira AL, Barbosa CR, Rocha OL. Study of electrochemical corrosion in samples of a horizontally solidified AlCuSi alloy. Int J Met Cast. 2022;16(3):1191-205. http://doi.org/10.1007/s40962-021-00657-w.
8. Soares DL, Barros AS, Dias M, Moreira AL, Cardoso JCA Fo, Silva AP, et al. The role of thermal and microstructural parameters on corrosion resistance of Unsteady-State horizontally solidified aluminum-copper hypoeutectic alloys. Int J Electrochem Sci. 2017;12(1):413-28. http://doi.org/10.20964/2017.01.63.
9. Rodrigues AV, Lima TS, Vida TA, Brito C, Garcia A, Cheung N. Microstructure and tensile/corrosion properties relationships of directionally solidified Al–Cu–Ni Alloys. Met Mater Int. 2018;24(5):1058-76. http://doi.org/10.1007/s12540-018-0116-5.
10. Santos HO, Reis FM, Kunioshi CT, Rossi JL, Costa I. Corrosion performance of Al-Si-Cu hypereutectic alloys in a synthetic condensed automotive solution. Mater Res. 2005;8(2):155-9. http://doi.org/10.1590/S1516-14392005000200011.
11. Kaufman JG, Rooy EL, editors. Aluminum alloy casting: properties, process, and applications. Ohio: ASM International; 2004. http://doi.org/10.31399/asm.tb.aacppa.9781627083355.
12. Osório WR, Spinelli JE, Ferreira IL, Garcia A. The roles of macrosegregation and of dendritic array spacings on the electrochemical behavior of an Al-4.5 wt.% Cu alloy. Electrochim Acta. 2007;52(9):3265-73. http://doi.org/10.1016/j.electacta.2006.10.004.
13. Brito C, Vida T, Freitas E, Cheung N, Spinelli JE, Garcia A. Cellular/dendritic arrays and intermetallic phases affecting corrosion and mechanical resistances of an Al-Mg-Si alloy. J Alloys Compd. 2016;673:220-30. http://doi.org/10.1016/j.jallcom.2016.02.161.
14. Qin Y-F, Wang S-Q. Ab-initio study of the role of Mg_2Si and Al_2CuMg phases in electrochemical corrosion of Al alloys. J Electrochem Soc. 2015;162(9):C503-8. http://doi.org/10.1149/2.0311509jes.
15. Al-Otaibi MS, Al-Mayouf AM, Khan M, Mousa AA, Al-Mazroa SA, Alkhathlan HZ. Corrosion inhibitory action of some plant extracts on the corrosion of mild steel in acidic media. Arab J Chem. 2014;7(3):340-6. http://doi.org/10.1016/j.arabjc.2012.01.015.
16. El-Sayed A, Mohamed AE, Hassan FSM, El-Mahdy MS. Influence of Titanium additions to Aluminum on the microhardness value and electrochemical behavior of synthesized Aluminum-Titanium alloy in solutions of HCl and H_3PO_4. J Mater Eng Perform. 2023;32(4):1760-77. http://doi.org/10.1007/s11665-022-07248-8.
17. Reddy L, Sattari M, Davis CJ, Shipway PH, Halvarsson M, Hussain T. Influence of KCl and HCl on a laser clad FeCrAl alloy: in-situ SEM and controlled environment high temperature corrosion. Corros Sci. 2019;158:108076. http://doi.org/10.1016/j.corsci.2019.07.003.
18. Wint N, Eaves D, Michailidou E, Bennett A, Searle JR, Williams G, et al. The kinetics and mechanism of filiform corrosion occurring on zinc aluminium-magnesium coated steel. Corros Sci. 2019;158:108073. http://doi.org/10.1016/j.corsci.2019.06.028.
19. Umoren SA, Eduok UM, Solomon MM, Udoh AP. Corrosion inhibition by leaves and stem extracts of *Sida acuta* for mild steel in 1 M H_2SO_4 solutions investigated by chemical and spectroscopic techniques. Arab J Chem. 2016;9(1):S209-24. http://doi.org/10.1016/j.arabjc.2011.03.008.
20. Saeed MT, Saleem M, Usmani S, Malik IA, Al-Shammari FA, Deen KM. Corrosion inhibition of mild steel in 1 M HCl by sweet melon peel extract. J King Saud Univ Sci. 2019;31(4):1344-51. http://doi.org/10.1016/j.jksus.2019.01.013.
21. Alaneme KK, Olusegun SJ, Alo AW. Corrosion inhibitory properties of elephant grass (*Pennisetum purpureum*) extract: effect on mild steel corrosion in 1 M HCl solution. Alex Eng J. 2016;55(2):1069-76. http://doi.org/10.1016/j.aej.2016.03.012.
22. Chaubey N, Savita, Singh VK, Quraishi MA. Corrosion inhibition performance of different bark extracts on Aluminium in alkaline solution. J Assoc Arab Univ Basic Appl Sci. 2017;22(1):38-44. http://doi.org/10.1016/j.jaubas.2015.12.003.
23. Kamal C, Sethuraman MG. Spirulina platensis: a novel green inhibitor for acid corrosion of mild steel. Arab J Chem. 2012;5(2):155-61. http://doi.org/10.1016/j.arabjc.2010.08.006.
24. Hazwan HM, Jain KM, Razali NN, Dahon NH, Nasshorudin D. The effect of *Tinospora crispa* extracts as a natural mild steel corrosion inhibitor in 1 M HCl solution. Arab J Chem. 2016;9(1):S616-24.
25. Reena KPD, Nayak J, Nityananda SA. Corrosion behavior of 6061/Al-15 vol. pct. SiC(p) composite and the base alloy in sodium hydroxide solution. Arab J Chem. 2016;9(2):S1144-54. http://doi.org/10.1016/j.arabjc.2011.12.003.
26. Prabhu D, Rao P. Corrosion behaviour of 6063 Aluminium alloy in acidic and in alkaline media. Arab J Chem. 2017;10(2):S2234-44.
27. Preethi KP, Shetty P, Rao SA. Electrochemical measurements for the corrosion inhibition of mild steel in 1 M hydrochloric acid by using an aromatic hydrazide derivative. Arab J Chem. 2017;10(5):653-63. http://doi.org/10.1016/j.arabjc.2014.09.005.
28. Xhanari K, Finsgar M. Organic corrosion inhibitors for Aluminum and its alloys in chloride and alkaline solutions: a review.

Arab J Chem. 2019;12(8):4646-63. http://doi.org/10.1016/j.arabjc.2016.08.009.
29. Loto RT. Surface coverage and corrosion inhibition effect of Rosmarinus officinalis and zinc oxide on the electrochemical performance of low carbon steel in dilute acid solutions. Results Phys. 2018;8:172-9. http://doi.org/10.1016/j.rinp.2017.12.003.
30. Bodunrin MO, Alaneme KK, Chown LH. Aluminium matrix hybrid composites: a review of reinforcement philosophies; mechanical, corrosion and tribological characteristics. J Mater Res Technol. 2015;4(4):434-45. http://doi.org/10.1016/j.jmrt.2015.05.003.
31. Fayomi OSI, Fayomi J, Elemike EE. Data onanti-corrosion characteristics of eco-friendly inhibitive extract on the hot corrosion degradation trend of A6063 Aluminum alloyin 1.0 M HCl solution. Data Brief. 2018;19:2468-76. http://doi.org/10.1016/j.dib.2018.04.007.
32. Liu Q, Cheng W, Zhang H, Xu C, Zhang J. The role of Ca on the microstructure and corrosion behavior of Mg–8Sn–1Al–1Zn–Ca alloys. J Alloys Compd. 2014;590:162-7. http://doi.org/10.1016/j.jallcom.2013.12.077.
33. Nikseresht Z, Karimzadeh F, Golozar MA, Heidarbeigy M. Effect of heat treatment on microstructure and corrosion behavior of Al6061 alloy weldment. Mater Des. 2010;31(5):2643-8. http://doi.org/10.1016/j.matdes.2009.12.001.
34. Zhang L, Jia R, Li D, Zhang W, Guo F. Effect of intermetallic phases on corrosion initiation of AZ91 alloy with rare earth Y addition. J Mater Sci Technol. 2015;31(5):504-11. http://doi.org/10.1016/j.jmst.2014.09.018.
35. Ares AE, Gassa LM, Gueijman SF, Schvezov CE. Correlation between thermal parameters, structures, dendritic spacing and corrosion behavior of Zn–Al alloys with columnar to equiaxed transition. J Cryst Growth. 2008;310(7-9):1355-61. http://doi.org/10.1016/j.jcrysgro.2007.11.169.
36. Ares AE, Gassa LM, Schvezov CE, Rosenberger MR. Corrosion and wear resistance of hypoeutectic Zn-Al alloys as a function of structural features. Mater Chem Phys. 2012;136(2-3):394-414. http://doi.org/10.1016/j.matchemphys.2012.06.065.
37. Belkhaouda M, Bazzi L, Salghi R, Jbara O, Benlhachmi A, Hammouti B, et al. Effect of the heat treatment on the behaviour of the corrosion and passivation of 3003 aluminium alloy in synthetic solution. J Mater Environ Sci. 2010;1(1):25-33.
38. Chaubey N, Yadav DK, Singh VK, Quraishi MA. A comparative study of leaves extracts for corrosion inhibition effect on aluminium alloy in alkaline medium. Ain Shams Eng J. 2017;8(4):673-82. http://doi.org/10.1016/j.asej.2015.08.020.
39. Buchheit RG. A compilation of corrosion potentials reported for intermetallic phases in aluminum alloys. J Electrochem Soc. 1995;142(11):3994-6. http://doi.org/10.1149/1.2048447.
40. Birbilis N, Buchheit RG. Electrochemical characteristics of intermetallic phases in aluminum alloys. J Electrochem Soc. 2005;152(4):B140-51. http://doi.org/10.1149/1.1869984.
41. Chaubey N, Singh VK, Quraishi MA. Papaya peel extract as potential corrosion inhibitor for Aluminium alloy in 1 M HCl: electrochemical and quantum chemical study. Ain Shams Eng J. 2018;9(4):1131-40. http://doi.org/10.1016/j.asej.2016.04.010.
42. Mendes G, Azevedo H, Dillon T, Rodrigues H, Hoffmann E, Rocha O. The Cu/Nb ratio influencing microstructure, mechanical and electrical properties in As-cast Al-3Cu-xNb alloys. Trans Indian Inst Met. 2023;76(6):1453-65. http://doi.org/10.1007/s12666-022-02863-4.
43. Dillon T, Mendes G, Azevedo H, Rodrigues H, Pereira P, Rocha O. Effects of growth and cooling rates via horizontal solidification of an AlCuNb Alloy: A thermal, microstructural and mechanical analysis. Trans Indian Inst Met. 2022;75(6):1429-39. http://doi.org/10.1007/s12666-021-02501-5.
44. Munöz AI, Mischler S, Interactive effects of Al buminand Phosphate ionson the corrosion of CoCrMo implant alloy. J Electrochem Soc. 2007;154:C562. https://doi.org/10.1149/1.2764238.
45. Arockiasamy A, Eliezer D, Wang PT, Horstemeyer MF, King RL. Effect of cathodic charging on Al-32Si-2Cu alloy in acidic solution. Mater Res. 2010;13(3):361-7. http://doi.org/10.1590/S1516-14392010000300014.
46. Osório WR, Siqueira CA, Santos CA, Garcia A. The correlation between electrochemical corrosion resistance and mechanical strength of As-cast Al-Cu and Al-Si alloys. Int J Electrochem Sci. 2011;6(12):6275-89. http://doi.org/10.1016/S1452-3981(23)19680-5.
47. Hua Q, Zeng Y, He Z, Xu Q, Min Y. Microstructure, synergistic mechanism and corrosion behavior of tin oxide conversion film modified by chitosan on Aluminum alloy surface. Colloid Interface Sci Commun. 2020;36:100262. http://doi.org/10.1016/j.colcom.2020.100262.
48. Osório WR, Peixoto LC, Moutinho DJ, Gomes LG, Ferreira IL, Garcia A. Corrosion resistance of directionally solidified Al–6Cu–1Si and Al–8Cu–3Si alloys castings. Mater Des. 2011;32(7):3832-7. http://doi.org/10.1016/j.matdes.2011.03.013.
49. Zavaleta-Gutierrez NE, Polo-Briceño ERP, Ñique-Gutierrez ND, Cicco H. Efecto del tratamiento térmico sobre la resistencia mecánica, corrosión intergranular y exfoliación de la aleación de Aluminio 7075. Materia. 2018;23(2):1-13. http://doi.org/10.1590/s1517-707620180002.0337.
50. Azevedo HM, Mendes GH, Rodrigues HR, Rocha FS, Costa TS, Moreira AL, et al. Effects of solidification, solution and aging processes on an AlCuNb alloy: thermal and microstructural analysis, microhardness, electrical resistivity and conductivity. J Therm Anal Calorim. 2024;149(3):953-66. http://doi.org/10.1007/s10973-023-12739-4.
51. Coutinho MM, Silva JIS, Sousa TP, Rosa DM. Upward unsteady-state solidification of dilute Al–Nb alloys: microstructure characterization, microhardness, dynamic modulusof elasticity, damping, and XRD analyses. Metals. 2019;713(9):1-15.